IEEE Access
Multidisciplinary ⋮ Rapid Review ⋮ Open Access Journal

Received February 13, 2020, accepted February 25, 2020, date of publication March 3, 2020, date of current version March 17, 2020.

Digital Object Identifier 10.1109/ACCESS.2020.2977921

Multi-Objective Optimal Dispatching for a Grid-Connected Micro-Grid Considering Wind Power Forecasting Probability

SIZHOU SUN[1,2], JINGQI FU[2], LISHENG WEI[1], AND ANG LI[2]
[1]Anhui Key Laboratory of Electric Drive and Control, Anhui Polytechnic University, Wuhu 241000, China
[2]School of Mechatronic Engineering and Automation, Shanghai University, Shanghai 200072, China

Corresponding author: Jingqi Fu (jqfu@staff.shu.edu.cn)

This work was supported in part by the Open Research Fund of Wanjiang Collaborative Innovation Center for High-End Manufacturing Equipment, Anhui Polytechnic University, under Grant GCKJ2018010 and Grant GCKJ2018013, and in part by the Natural Science Foundation of Anhui Province under Grant 1608085MF146.

ABSTRACT In recent years, a large number of wind power has been applied in the micro-grid (MG). Influenced by randomness characteristics of wind speed, the uncertainty in the power output of wind turbines imposes some safety and stability problems on the optimal energy management in MG. To address this problem, an expert energy management system (EEMS) considering wind power probability is developed in this study for optimal dispatching of a typical grid-connected MG. The EEMS composes of wind power probabilistic forecasting module, multi-objective optimization module and energy storage system (ESS) module. In the wind power forecasting module, wind power probabilistic forecasting based on complementary ensemble empirical mode decomposition with adaptive noise (CEEMDAN) and Gaussian process regression (GPR) is proposed in this study. To improve the forecasting results, CEEMDAN, an effective signal processing method, is employed to decompose the wind power data, then, the decomposed subseries are utilized as the inputs of GPR for probabilistic forecasting. A two-step solution methodology combining an efficient and effective improved multi-objective bat algorithm (IMOBA) with fuzzy set theory (FST) is put forward to solve the optimal dispatching problems. In the first step, IMOBA is developed to optimize the energy dispatching of EEMS by minimizing both economic cost and pollutant emissions simultaneously, and obtain a well-distributed set of Pareto optimal front (POF), then, FST is employed to identify the best compromise solutions from POF. Six operational scenarios of a typical grid-connected MG based one-POF-one-day and one-POF-one-hour dispatching schemes are constructed to investigate the effectiveness of the proposed strategy and provide more flexibility for decision makers. The results illustrate that EEMS can effectively schedule power generation and energy storage by considering economic cost and pollutant emission objectives simultaneously.

INDEX TERMS Wind power probabilistic forecasting, multi-objective optimization, micro-grids, bat algorithm, expert energy management system.

I. INTRODUCTION

Environmental pollution and greenhouse effect caused by consumption of fossil fuel resources, diminution of conventional energy resources, and security caused by long distance electric power transmission, and bulk electric power transformation promote the wide development and application of renewable-energy-based micro-grid (MG) in the vicinity of electric power consumers. To avoid the risk of the exhaustion of fossil energy and deal with global climate change, renewable energies, mainly including wind power, solar energy and so on, have been vigorously developed as main parts of MG system in recent years, which has been the common consensus of the scientific community [1]. Apart from wind power and photovoltaics (PV), micro-turbines (MTs), fuel cell (FC), and other distributed generators (DGs) have been also widely utilized in MG system with energy storage system (ESS). As the randomness and fluctuations of wind power and other

The associate editor coordinating the review of this manuscript and approving it for publication was Yang Li.

renewable energy, the renewable energy-based MG accompanies with uncertainty. For MG system operator, the wind power forecasting (WPF) values and their uncertainty are an important factor for scheduling. This uncertainty information is beneficial for the optimal scheduling of ESS as well as determining the requirement to compensate the WPF errors. Dispatching management of MG is an energy optimal set points problem under the technical and economic constraints [2]. The generation capacities of DGs including wind turbines (WT) are prerequisites for the MG scheduling. Thus, WPF is one of the important tasks that should be considered in advance for the optimal dispatching of MG [3].

In recent years, many studies on optimal dispatching of MG considering wind energy uncertainty have been executed. A multi-objective method for the short-term active power optimal dispatching of a stand-alone MG is developed in Ref. [4], where the wind power and solar power with uncertainties for various possible scenarios are modeled using fuzzy sets, and adaptive chaos clonal evolutionary programming method is utilized to deal with the optimal dispatching. A similar problem is solved in Refs. [2], [5], where wind power and solar power are modeled by Weibull function and Beta probability distribution functions, respectively. To deal with the uncertainties of wind power, some researchers have developed various WPF models for optimal energy dispatching of wind turbines in MG [6], [7]. In Ref. [6], wavelet decomposition signal processing method was used to decompose the wind speed time series, then the decomposed results were employed as the inputs of artificial neural network for wind speed forecasting, then, adaptive probabilistic concept of confidence interval approach was applied to address the uncertainty problems of wind power. Most of WPF approaches yield deterministic forecasting [8], [9], no matter how much the forecasting accuracy of wind power deterministic prediction model is, there still exist some uncertainty components, thus cannot provide the uncertainty information about wind power [10], [11]. Thus, in recent years, wind power probabilistic forecasting models have been developed to provide uncertainty information for studying the optimal energy management [12], [13]. In Ref. [12], wind power probabilistic forecasting were obtained by using kernel density estimator (KDE) according to rolling process and the forecasting results were applied in optimal scheduling of gas-fired generators.

ESS, an important part in MG, can compensate and eliminate the fluctuation of renewable energy, thus improving the operational performance of MG [14]–[16]. Ref. [14] proposed a new modeling approach to optimize the energy management of a MG with multiple energy carrier. The modeling approach also contains 24h ahead power forecasting module for estimation of the electrical and thermal loads and the output of wind turbines, then particle swarm optimization (PSO) algorithm was developed to solve the energy optimization problems. Ref. [15] proposed a building based virtual ESS for eliminating the daily operating cost of hybrid energy MG. Ref. [17] presented an intelligent optimization model for energy management system (EMS) in MG using recurrent neural network (RNN). The RNN and additional indices were employed to evaluate demand response (DR) of customers, and ant-lion optimization (ALO) algorithm was developed to determine the optimal set points of power generation, energy storage, and responsive load offers for minimizing production cost and better utilizing renewable energy resources.

Although EMS in the above literatures obtain good optimal dispatching results, however, these approaches only consider economic operational cost. Pollutant emission pollutes the environment and affects people's health. Thus, pollutant emission is another indispensable objective that should be considered in the optimal energy dispatching of MG. As net pollutant emission and operational cost are two conflicting objectives, many multi-objective models have been developed to solve these problems simultaneously [7], [18]–[20]. In Ref. [7], multi-objective bacterial foraging optimization (MOBF) was developed to determine the optimal system configuration and an interactive fuzzy satisfying (IFS) technique was utilized to realize the tradeoff between operational cost and environment impacts for optimal dispatching of MG. In Ref. [18], multi-objective uniform water cycle algorithm was developed to optimize the short-term operational management of MG for obtaining pareto optimal fronts (POF) and an interactive process is employed to make a compromise between the two conflicting objectives. In Ref. [19], multi-objective PSO algorithm was developed to optimize the dispatching of an off-grid hybrid micro-grid system for yielding the optimal system configuration. After multi-objective optimization, the optimal hybrid MG system was obtained by determining the tradeoff between reliability, cost, and environmental impact. In Ref. [21], a multi-objective bi-level operation model was proposed to optimize the dispatching of the distribution network with grid-connected microgrid by self-adaptive genetic algorithm (GA) and non-linear programming. A multi-objective dynamic optimal dispatching model for isolated microgrids was developed to coordinate multiple different optimization objectives, including economic cost, environmental factors, and users experience, using θ-dominance based evolutionary algorithm [22]. As the above-mentioned studies, multi-objective optimization results for energy management of MG are a set of Pareto solutions, and one solution which compromises multi-objectives needs to be determined.

However, there still exist some research gaps in the similar study domain. (i) Deterministic wind power forecasting is obtained by artificial neural network combined with signal decomposition method, or wind power data are determined by Weibull function. But probabilistic wind power forecasting directly obtained by artificial intelligent approach with signal decomposition technique may be preferable option for its quick response and lower cost [12]. (ii) In previous literatures, optimal hourly dispatching over 24h a day is generally made by one-POF-per-day scheme for multi-objective optimization, in addition, only three scenarios considering operational cost objective, environmental factor objective or

both operational cost and environmental factor objectives, are developed to investigate the energy management of MG, which may not meet the diverse needs of decision makers. (iii) In practical applications, it is a tricky issue to determine the best compromise solutions from the generated numerable POFs, and decision makers often have not deterministic consistent solutions for the actual MG operational requirements.

To solve the above problems, an expert energy management system (EEMS) is proposed for grid-connected MG using a multi-objective optimization model and the main works and contributions of this study can be summarized as follows.

(i) *Dispatching Model:* In this study, EEMS considering wind power probability for a grid-connected MG is proposed. The studying grid-connected MG contains WTs, PV, FC, MT, and lead acid battery pack (namely ESS), while EEMS includes WPF module, multi-objective optimization module, and ESS module. The aims of EEMS are to optimize the energy management of MG with respect to operational cost and pollutant emission objectives.

(ii) *Probabilistic Wind Power Forecasting:* A new compound model based on complementary ensemble empirical mode decomposition with adaptive noise (CEEMDAN) and Gaussian process regression (GPR) tuned by improved bat algorithm (IBA), namely CEEMDAN-IBA-GPR, is developed to generate probabilistic WPF values using historical actual wind power data by rolling process. In the proposed model, CEEMDAN divides the empirical wind power time series into a few intrinsic mode functions (IMFS) and one residual. GPR with inappropriate parameters may fall into over-fitting or under-fitting in training process, thus, hyper-parameters of GPR should be optimized for WPF. Chaos initialization of population, sine map mutation and adapting weight of global best are applied to improve the optimization performance of bat algorithm (BA), namely IBA, and IBA is compared with BA and PSO using testing functions Rosenbrock and Schaffer F6. Then, IBA is developed to tune the hyper-parameters in GPR model. The well-trained GPR model makes probabilistic wind power forecasting using the decomposed wind power data by rolling process. The probabilistic WPF results are utilized as one part in the MG system for optimal dispatching.

(iii) *Two-Step Solution Methodology:* A comprehensive formulation considering wind power probability and operational constraints is employed to model multi-objective optimal scheduling of MG. An improved multi-objective bat algorithm (IMOBA) is employed to optimally generate a well-distributed set of POFs in the first step, then, the best compromise solutions are determined from the entire POFs by fuzzy set theory (FST).

(iv) *Multi-Scenario Application:* Multiple operational scenarios of a typical grid-connected MG based on one-POF-per-day and one-POF-per-hour dispatching schemes provide more flexibility for decision makers to determine the preferred hourly optimal solutions. One-POF-per-hour operational dispatching scheme is designed to determine the optimal hourly energy set points, and the final multi-objective optimization solutions are obtained by aggregating the 24 primary objective values.

Apart from the above part, the remainders of this study are arranged as follows. Wind power probabilistic forecasting model based on CEEMDAN and GPR tuned by IBA is presented in Section II. The DGs and EMS in MG, the corresponding mathematical descriptions, and IMOBA for multi-objective energy optimization of EEMS are presented in Section III. In Section IV, the application of the proposed model in a typical MG and the simulation results are presented. In the end, conclusions are drawn in Section V.

II. WIND POWER FORECASTING

A. WIND POWER DECOMPOSITION METHOD

CEEMDAN approach developed based on empirical mode decomposition (EMD) and ensemble empirical mode decomposition (EEMD) has been successfully applied in fault feature extraction [23], fault diagnosis [24] and other time series processing [25], [26].

The basic principle of EMD approach is to break the complicated signal into a few small and more stable subseries, including IMFS and one residual (Res), by using the local characteristics of the signal [27], [28]. To eliminate the mode mixing caused by EMD, EEMD is developed by adding a white Gaussian noise-assisted signal in the original data during the decomposition process of EMD, then these noise-assisted signals are eliminated through summing the average. However, these noise-assisted signals cannot be completely eliminated after finite iteration [25], [26]. To eliminate the contamination of residual noise, CEEMDAN approach adds adaptive assisted-noise signals to the original data in the decomposition process of EMD. The working process of CEEMDAN can be briefly shown as the following steps.

Step 1 Assume that $p(t)$ is original wind power data, add white Gaussian noise $n(t)$ in the original wind power data by weighted coefficient ω_0 that adjusts the noise amplitude during iteration, expressed as Eq. (1).

$$P(t) = p(t) + \omega_0 \times n(t) \tag{1}$$

Step 2 Decompose the noise-assisted wind power data $P(t)$ by EMD method and obtain the first modes $IMF_1^i(t)$. Then, by the way of mean, the first mode of CEEMDAN is yielded, as shown in Eq. (2).

$$\overline{IMF_1^i(t)} = \frac{1}{L}\sum_{i=1}^{L} IMF_1^i(t) \tag{2}$$

Step 3 The first residual component $r_1(t)$ of CEEMDAN can be obtained according to Eq.(3).

$$r_1(t) = P(t) - \overline{IMF_1^i(t)} \tag{3}$$

Step 4 The second mode can be obtained by decomposing and averaging the first noise-added residual component $r_1(t) + \omega_1 \times E_1(n(t))$, expressed as Eq. (4).

$$\overline{IMF_2^i(t)} = \frac{1}{L}\sum_{i=1}^{L} E_1(r_1(t) + \omega_1 E_1(n(t))) \tag{4}$$

where $E_i()$ denotes the EMD decomposition function.

Step 5 The kth residual component $r_k(t)$ is obtained according to following Eq. (5).

$$r_k(t) = r_{k-1}(t) - \overline{IMF_k^i(t)}, \quad k = 2, 3, \cdots, K \tag{5}$$

Step 6 Obtain the kth IMF by the same decomposition means in Step 4, expressed as Eq. (6).

$$\overline{IMF_k^i(t)} = \frac{1}{L}\sum_{i=1}^{L} E_1(r_k(t) + \omega_k E_k(n(t))) \tag{6}$$

Step 7 Repeat Steps 5 $\sim$ 6 until the residual component becomes a monotonic function. In the end, the final decomposed results of wind power data are obtained as Eq. (7).

$$v(t) = \sum_{i=1}^{K} \overline{IMF_i(t)} + r_k \tag{7}$$

B. GAUSSIAN PROCESS REGRESSION (GPR)

GPR, a powerful probabilistic and Bayesian nonparametric method, can provide WPF probabilistic distribution rather than deterministic forecasting values [29], [30]. Supposed a sample set $D = (x_i, y_i)$, where $n = 1, 2, \cdots, N$, x_i is the input variable and $x_i \epsilon R_N$, y_n is the corresponding output variable, whose joint probabilistic distribution follows n-dimension Gaussian distribution and $y_i \epsilon R$. $X = [x_1, x_2, \cdots, x_N]^T$, $Y = [y_1, y_2, \cdots, y_N]^T$. GPR is defined as $f(x) \sim Gp(m(x), k(x, x'))$, as shown in Eq. (8).

$$\begin{cases} m(x) = E[f(x)] \\ k(x, x') = E[(f(x) - m(x)), (f(x') - m(x')] \end{cases} \tag{8}$$

The standard linear regression model with Gauss white noise can be expressed as Eq. (9).

$$y = f(X) + \varepsilon \tag{9}$$

where ε denotes independent random Gaussian noise variable with zero mean variance, which is expressed as Eq. (10).

$$\varepsilon \sim N(0, \delta_n^2) \tag{10}$$

where δ_n^2 denotes variance.

From the independent identically distributed noise assumption, ε and $\varepsilon*$ are stated as Eq.(11).

$$\begin{bmatrix} \varepsilon \\ \varepsilon_* \end{bmatrix} \sim N\left(0, \begin{bmatrix} \sigma_n^2 I & 0 \\ 0 & \sigma_n^2 I \end{bmatrix}\right) \tag{11}$$

In the GPR definition, the predicted output from the posterior distribution function can be obtained using the Bayesian framework. The joint Gaussian prior distribution of the output y and y^* are shown in Eq.(12).

$$\begin{bmatrix} y \\ y^* \end{bmatrix} \sim N\left(0, \begin{bmatrix} C(X, X) + \sigma_n^2 I & C(X, x^*) \\ C(X, x^*) & C(x^*, x^*) \end{bmatrix}\right) \tag{12}$$

$$\begin{aligned} C(X, x^*) &= C(X, x^*)^T \\ &= [C(x_1, x^*), C(x_2, x^*), \cdots, C(x_n, x^*)] \end{aligned} \tag{13}$$

where $C(X, x^*) = C(x^*, X)^T$, which can be abbreviated as C^*, then the forecasting results for the testing samples is expressed as Eq. (14).

$$\hat{y} = C^{*T}(K + \sigma_n^2 I)^{-1} y \tag{14}$$

$\hat{y}$ follows normal distribution, whose mean value μ and covariance value σ are stated as Eq. (15).

$$\begin{cases} \mu_{\hat{y}} = C(x^*, X)[C(X, X) + \sigma_n^2 I]^{-1} y \\ \sigma_{\hat{y}} = C(x^*, x^*) - C^T(x^*, X)[C(X, X) + \sigma_n^2 I]^{-1} C(x^*, X) \end{cases} \tag{15}$$

The confidence interval is used to describe the probabilistic prediction results of the GPR model. The confidence interval of the predicted results is shown as Eq. (16).

$$\begin{aligned} &[Lb_{1-\alpha}(y'),\ Ub_{1-\alpha}(y')] \\ &\quad = \left[\mu_{y'} - z_{(1-\alpha)/2}\sigma_{y'}^2,\ \mu_{y'} + z_{(1-\alpha)/2}\sigma_{y'}^2\right] \end{aligned} \tag{16}$$

where $L_b(1-\alpha)(y')$ and $U_b(1-\alpha)(y')$ are the forecasting lower and upper bounds of the predicted values, respectively. $z(1-\alpha)/2$ stands for quantiles of standard normal distribution. Thus, $[L_b(1-\alpha)(y'), U_b(1-\alpha)(y')]$ is the forecasting probabilistic prediction interval.

The covariance function in GPR, satisfying Mercer condition, is a symmetric function and is positive definite in finite input set. Therefore, the covariance function can be equivalent to kernel function and Eq. (16) can be rewritten as Eq. (17).

$$\mu_{y^*} = \sum_{i}^{n} \alpha_i C(x^i, x^*) \tag{17}$$

where $\alpha = [C(X, X) + \sigma_n^2 I]^{-1} y$.

Square exponential kernels function (SEK) is adopted as the kernel function in GPR, which is expressed as Eq. (18). The forecasting mean values are to combine the kernel function linearly, which can map the nonlinear wind power data into high-dimension feature space and transfer into linear regression.

$$C_{Se} = \sigma_f^2 \exp(-\frac{(x^i - x^j)^2}{2\alpha\ell^2}) + \sigma_n^2 \delta^{ij} \tag{18}$$

where σ_f^2, α, ι, σ_n^2, and $\delta_{i,j}$ are signal variance, shape parameter of kernel function, relevant measured hyperparameters, noise variance and Kronecker signal, respectively.

C. WIND POWER PROBABILISTIC FORECASTING MODEL

CEEMDAN-IBA-GPR model is constructed to make 1-hour interval wind power probabilistic forecasting, which is shown

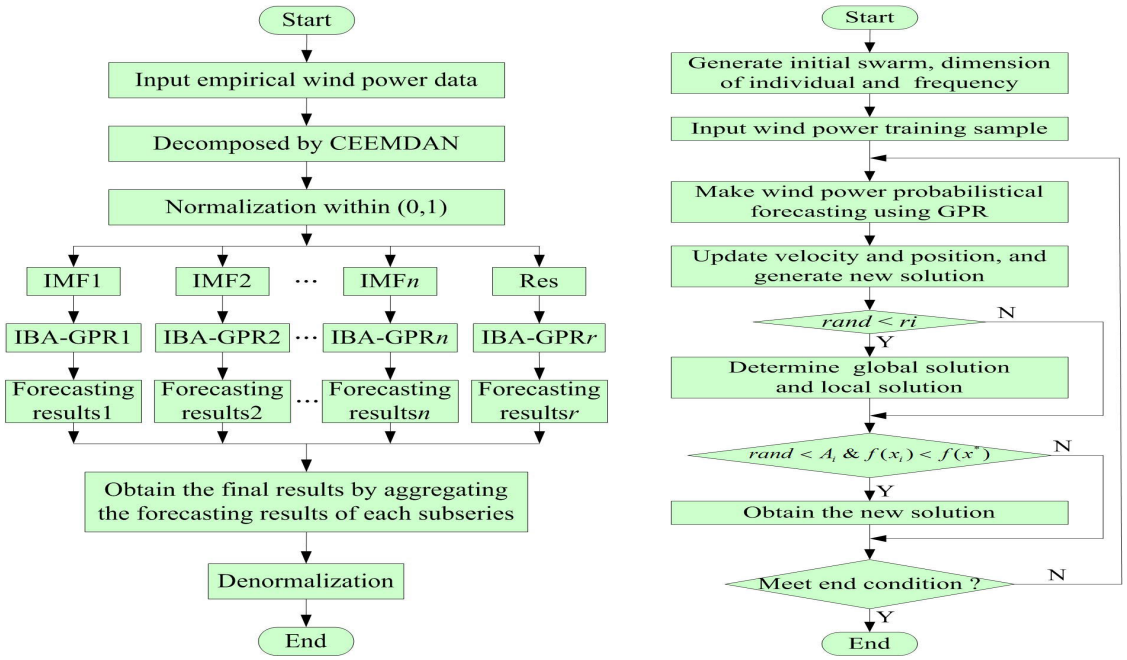

(a) Flowchart of CEEMD-IBA-GPR for WPF

(b) Flowchart of IBA-GPR

FIGURE 1. Wind power probabilistic forecasting model.

in Fig. 1 (a) and flowchart of IBA-GPR model for WPF is illustrated in Fig.1 (b). As seen from Fig. 1, the WPF model can be mainly divided into three stages, and the main working mechanisms are presented as follows.

Stage 1: Utilize CEEMDAN approach to break the original wind power empirical data into a few IMFs and one Res with different frequency and relatively stable features. In this stage, the training sample data is added adaptively weighted noise signal, then apply EMD to decompose the noise-assisted data, in the end, eliminate the noise signal by summing after the maximum iteration is reached.

Stage 2: After normalization within (0,1), train IBA-GPR using the decomposed subseries in this stage, which is shown in Fig.1 (b). In the training process, the function expressed as Eq.(19) is adopted as the fitness function to assess the forecasting results, and IBA approach optimizes hyper-parameters of GPR. After the maximum iteration, the global solution representing the hyper-parameters of GPR and well-trained IBA-GPRs are obtained.

$$f(x) = \exp[-0.005(\frac{\hat{x}(t) - x(t)}{x(t)} \times 100\%)] \quad (19)$$

where $\hat{x}(t)$ and $x(t)$ stand for the forecasting values and actual measured values, respectively.

Stage 3: Employ the well-trained IBA-GPRs to make wind power probabilistic forecasting. After denormalization, obtain the final WPF results by aggregating the forecasting results of each subseries.

D. EMPIRICAL WIND POWER SAMPLE DATA AND DECOMPOSITION

A hybrid model using historical wind power data is constructed in this study to predict future wind power probabilistic value. The historical wind power data are selected from the data store center of a wind farm located in east of China. The wind turbines are installed at the top of a mountain with approximately 150m where the wind power data are measured and collected every 10 minutes. One hour to several hours ahead time horizons WPF plays an important role in economic load dispatch and is beneficial for operation management [31]. In addition, it makes sense to investigate the role of the energy storage equipment and economic dispatch within a 24h time period [6], [32], thus, 24h ahead WPF is considered in this study, and these wind power data are converted to one-hour tick data by the mean of the consecutive 10-min tick data, which are shown in Fig. 2 and their statistical indices are displayed in Table 1. The first 1464 consecutive wind power data and the subsequent 24 consecutive data are utilized as the training samples and the test samples, respectively. The decompositions of wind

TABLE 1. Statistical description of the empirical wind power data (kW).

Samples	Number	Max	Min	Mean	Std.dev
Entire samples	1488	48.47	0.01	16.67	12.84
Training data	1464	48.47	0.01	16.65	12.93
Testing data	24	29.39	11	18.04	5.05

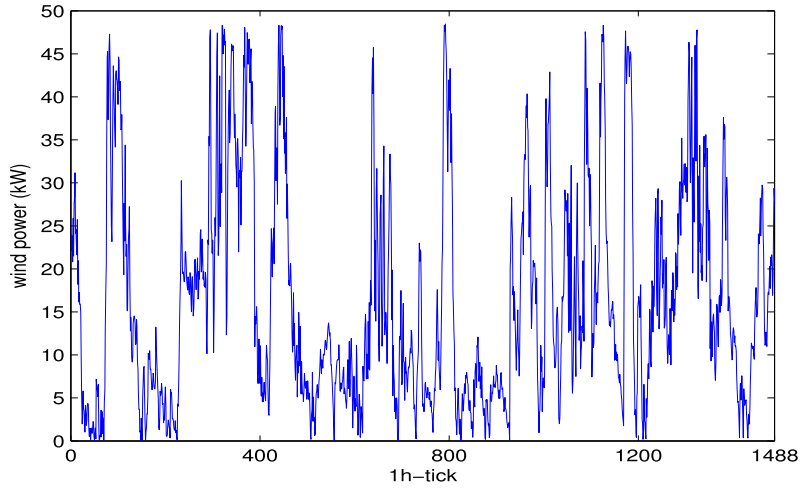

FIGURE 2. Historical wind power data.

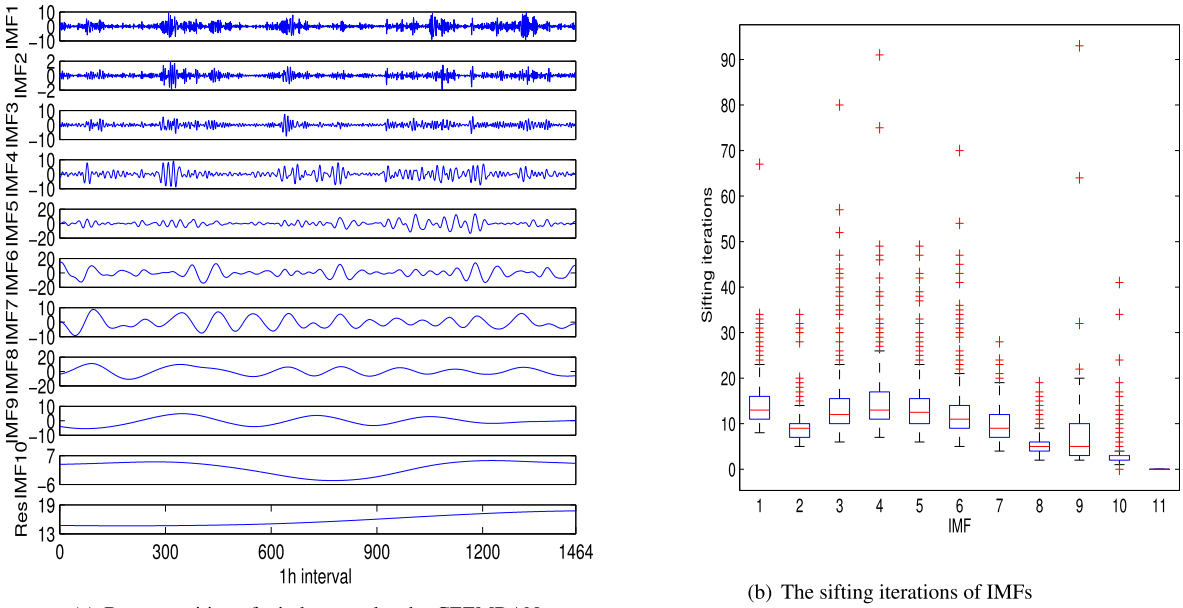

(a) Decomposition of wind power data by CEEMDAN

(b) The sifting iterations of IMFs

FIGURE 3. Decomposition of historical wind power data by CEEMDAN.

power data by CEEMDAN are presented in Fig. 3, and all the decomposed subseries show relative stability.

III. PROBLEM FORMULATION

A. MODELING OF MULTI-OBJECTIVE OPTIMIZATION PROBLEM

In this study, grid-connected MG system contains PV, WT, MT, FC and ESS, which are shown in Fig.4. As seen from the figure, DGs and grid have communication interfaces with EMS by dashed line. All the operation information of all the DGs and grid are transmitted to EMS, then, EMS determines the optimal set points to make power distribution by multi-objective optimization algorithm, thus, the total operation cost and the pollutant emission can be minimized simultaneously. Considering the small power demand, the short power wires, and a small amount application of advanced power electronic equipments, all the transmission loss is assumed as one part in the load.

At least two objectives with a few constraints in EEMS should be considered. The general formulation that determines the output shares of DGs is illustrated as follows.

1) OBJECTIVE FUNCTION

For the grid-connected MG, the total operation cost contains the fuel cost for power generator by MT, startup/shutdown cost, and charging/discharging cost by the ESS as well as the costs of the exchanging power with the connected power grid, which can be expressed mathematically as follows.

$$F_1 = \min \sum_{t=1}^{T} \sum_{j=1}^{3} C_j(t) \tag{20}$$

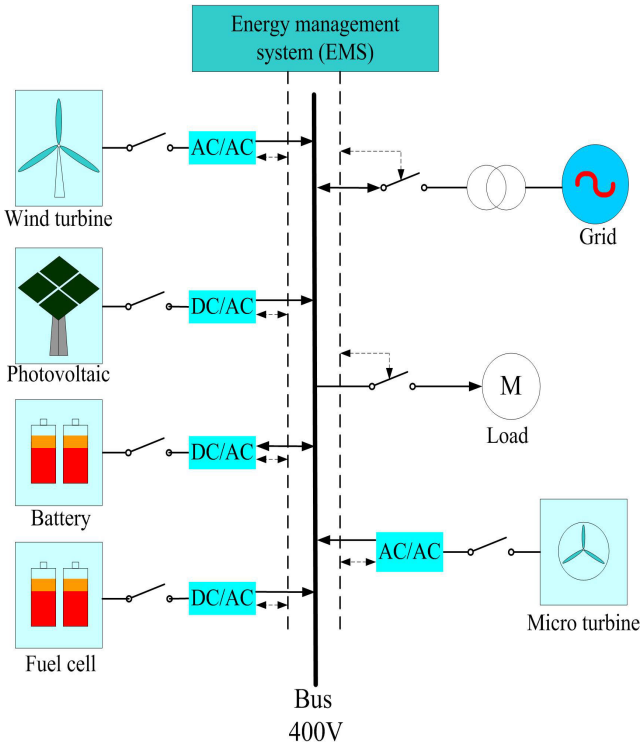

FIGURE 4. The structure of micro-grid system.

where $C_1 \sim C_3$ are expressed as follows.

$$C_1 = \sum_{i=1}^{N_1} [u_i(t)P_{gi}(B_{gi}(t)+K_{OMi})+S_{gi}|u_i(t)-u_i(t-1)|] \tag{21}$$

$$C_2(t) = \sum_{k=1}^{N_2} u_k(t)P_{sk}B_{sk}(t) \tag{22}$$

$$C_3(t) = P_{grid}(t)B_{grid}(t) \tag{23}$$

where N_1 and N_2 are the total quantity of the generators and the energy storage equipments, respectively. $B_{gi}(t)$, $B_{sk}(t)$, and $B_{grid}(t)$ represent the bids of the ith MT, kth energy storage equipment, and the utility at time t, respectively. $u_i(t)$ and $u_k(t)$ stand for the ON or OFF state of power generators and ESS, respectively. K_{OMi} denotes weighted coefficient. $P_{gi}(t)$ and $P_{sk}(t)$ are output power of ith generator and charge/discharge power of the kth battery pack, respectively. $P_{grid}(t)$ is the exchanging power between MG and the upstream grid. The emission objective function of the total pollutant mainly including sulfur dioxide (SO_2), carbon dioxide (CO_2) and nitrogen oxides (NO_x) can be expressed as Eq. (24).

$$F_2 = \min \sum_{t=1}^{T} \{(\sum_{i=1}^{N_3}\sum_{j=1}^{N_4} w_{i,j}P_{gi}(t) + S_{ei}(t)|u_i(t) - u_i(t-1)|) + \sum_{i}^{N_3} P_{grid}(t)w_{gridi}(t)\} \tag{24}$$

where $w_{i,j}$ and w_{grid} represent the emission factor for the ith generator and the utility, respectively. N_3 and N_4 denote the kind of emission (SO_2, CO_2 or NO_x) and the total quantity of pollutant generators, respectively. Thus, the formulation of multi-objective optimization is expressed as $min[F_1, F_2]$, however, the operation cost and pollutant emission are two conflicting objectives.

2) CONSTRAINTS

a: POWER BALANCE

The total electrical power supplied by MT, FC, PV, WT, ESS and the connected power system must be equal to the load demand, as shown in Eq. (25).

$$\sum_{i=1}^{N_1} P_w(t) + \sum_{i=1}^{N_2} P_p(t) + \sum_{i=1}^{N_3} P_m(t) + \sum_{i=1}^{N_4} P_f(t) + \sum_{i=1}^{N_5} P_e(t) + P_G(t) = \sum_{i=1}^{N_6} P_L(t) \tag{25}$$

where $P_w(t)$, $P_p(t)$, $P_m(t)$, $P_f(t)$, $P_e(t)$ and $P_L(t)$ denote the output power of the WT, PV, MT, FC, ESS, and load at time t, respectively. $P_G(t)$ represents the interaction power between MG and the public grid.

b: POWER SUPPLY CAPACITY

Each unit can supply power within its specific power range, which is explained as Eq. (26).

$$\begin{cases} P_{gi,min}(t) \le P_{gi}(t) \le P_{gi,max}(t) \\ |P_{Grid}(t)| \le P_{exgrid,max}(t) \end{cases} \tag{26}$$

where $P_{gi,max}$ and $P_{gi,min}$ stand for the maximum and the minimum supply power of the ith generator, respectively. $P_{exgrid,max}$ denotes the maximum power that is exchanged between the upstream power system and MG.

c: ENERGY STORAGE LIMITS

Batteries in ESS continuously charges and discharges during the operation of microgrid, which should obey the limitation of the charge and discharge rate, as expressed as Eqs. (27) and (28).

$$\begin{cases} E_k(t) = E_k(t-1) + P_c(t)\Delta t\eta_c \\ E_k(t) = E_k(t-1) - \dfrac{P_d(t)\Delta t}{\eta_d} \end{cases} \tag{27}$$

where η_c and η_d are the charge and discharge rate, respectively, and $\eta_c = \eta_d$ =0.9. P_c and P_d are the charge and discharge power, respectively, and Δt denotes the time interval.

$$E_{k,min}(t) - E(0) \le E_k(t) \le E_{k,max} - E(0) \tag{28}$$

The formulation illustrates that ESS compensates the fluctuation of the renewable resources with the limitation range. $E_{k,max}$, $E_{k,min}$ and $E(0)$ are set as 150kW, -150kW and 5kW, respectively.

B. THE SOLVING METHOD OF THE MULTI-OBJECTIVE OPTIMIZATION

It is easy to obtain the solution using one criterion when only one objective solution in single-objective optimization problem should be optimized. However, in multi–objective optimization problem, more than one criterion for optimization under conflicting targets needs to be solved simultaneously, thus, there exists a POF solution set [7], [33]. The multi-objective optimization problem can be equivalent to minimization problem expressed as Eqs. (29) and (30).

$$minimize: F(x) = \{f_1(x), f_2(x), f_3(x), \cdots\cdots f_n(x)\} \quad (29)$$

$$st: \begin{cases} k_i(x) \geq 0 & i = 1, 2, \cdots n_1 \\ g_i(x) = 0 & i = 1, 2, \cdots n_2 \\ h_i(x) \leq 0 & i = 1, 2, \cdots n_3 \end{cases} \quad (30)$$

where n, n_1, n_2, n_3 denote the quantity of the objective functions and the corresponding constraints functions.

Pareto Dominance: Assumed two vectors x and y, x is named to dominate y if and only if:

$$\begin{cases} f_i(x) \leq f_i(y) & \forall i \in \{1, 2, \cdots N\} \\ f_i(x) < f_i(y) & \exists i \in \{1, 2, \cdots N\} \end{cases} \quad (31)$$

where N stands for the number of subobjective functions.

Pareto Optimal Front (POF):

In a decision vector space Ω, there are not any vector u optimal than v, in the other words, $\forall u \in \Omega$, not exist $u \prec v$, then, v is named as Pareto optimality. A set consisting of the Pareto optimality is defined as POF.

Optimal Compromise Solution

After determination of POF solution set, fuzzy set theory (FST) [34] is employed to identify the best solution of the multi-objective optimization problem. In the method, each objective function is set as imprecise or fuzzy goal, then, these goals are quantified by their membership functions expressed as Eq. (32).

$$\mu_n = \begin{cases} 1 & f_n \leq f_{nmin} \\ \dfrac{f_{nmax} - f_n}{f_{nmax} - f_{nmin}} & f_{nmin} \leq f_n \leq f_{nmax} \\ 0 & f_n \geq f_{nmax} \end{cases} \quad (32)$$

where f_n, f_{nmax} and f_{nmin} are the nth objective function, the maximum and minimum of the nth objective function, respectively, $n \in \{1, 2 \cdots N\}$. Standardized satisfaction μ^k of each noninferior solution, expressed as Eq. (33), can be obtained according to Eq. (32).

$$\mu^k = \frac{\sum_{n=1}^{N} \mu_n^k}{\sum_{k=1}^{K} \sum_{n=1}^{N} \mu_n^k} \quad (33)$$

where K denotes the number of noninferior solution. The maximum standardized satisfaction of the noninferior solutions can be determined as the optimal compromise solution.

C. OPTIMIZATION ALGORITHM FOR MULTI-OBJECTIVE OPTIMIZATION PROBLEM IN MG

Multi-objective bat algorithm (MOBA) was firstly developed by Yang [35] to solve multi-objective optimization problem using the echolocation features and frequency tuning technique of micro bats. The optimization performance of MOBA has been validated by Zitzler-Deb-Thiele's functions No. 1 $\sim$ 3 [10]. MOBA has been successfully applied in solving welded beam design [35], shell and tube heat exchanging [36], security and quality of service in a real-time operating system [37], and other multi-objective optimization problems [38]. However, the application of MOBA in the energy management system of MG has not been taken seriously, thus, a multi-objective optimization model based improved MOBA (IMOBA) is developed for the EEMS of MG in this study.

1) BAT ALGORITHM

BA is a new metaheuristic optimization algorithm that emulates the phenomenon of echolocation of a bat during flights. The bats have capacity in emitting sound pulses at approximately 20 kHz frequency that exceeds the limits of human hearing ability. By adjusting the pulse frequency, a bat can precisely avoid any obstacles and determine the dynamic spatial position of an object [39]. The working process of BA is shown as follows.

(i) *Initialization:* To apply BA, the initial velocity, position, and frequency of bats are randomly initialized within the feasible solution range.

(ii) *Bat Motion:* In a D-dimension feasible search solution space, the velocity $v_i(t)$, position $x_i(t)$, and frequency r_i are calculated and updated as follows.

$$r_i = r_{\min} + (r_{\max} - r_{\min})\beta \quad (34)$$

$$v_i(t+1) = v_i(t) + (x_i(t) - x^*)r_i \quad (35)$$

$$x_i(t+1) = x_i(t) + v_i(t+1) \quad (36)$$

where β denotes a random value within (0,1) and x^* stands for the best global solution at the current iteration. From Eq. (34), it can be obtained that the frequency is only a factor that influences the step magnitude of each individual at each iteration.

(iii) *New Solution Generation:* By a random walk, each bat generates a new solution in the local search, which is expressed as Eq. (37).

$$x_{new} = x_{old} + \mu \cdot A(t) \quad (37)$$

where μ stands for a random value within (0,1) and $A(t)$ denotes the average values of individuals' loudness at the tth iteration.

(iv) *Loudness and Pulse Emission:* Loudness and pulse emission change and update with the procedure of catching prey. At the beginning of foraging, bats emit high volume loudness and low frequency pulses. After prey has been found, the volume of loudness decreases while pulse rate increases. The prey procedure can be

mathematically express as follows.

$$A_i(t+1) = \theta \cdot A_i(t) \tag{38}$$

$$r_i(t) = r^0[1 - \exp(-\eta t)] \tag{39}$$

where η and θ are constants, $A_i(t)$ and r_i are the loudness and the emission rate of pulse at the tth iteration.

(v) Repeat Step *ii* ∼ *iv* until the end condition is satisfied and the optimal solution can be obtained.

2) IMPROVED BAT ALGORITHM

The initial population in the standard BA are generated randomly, the uneven distribution and lack of mutation mechanism might cause premature convergence and the population fall into local optimum easily. Chaos is a special aperiodic motion approach of nonlinear system and Chaos is introduced to produce the initial population in BA by using its characteristics of randomness, ergodicity and sensitivity to initial parameters. Logical self-mapping function with good ergodicity capacity, a good Chaos function [40], [41], is used to improve global search ability of BA approach, which is mathematically expressed as follows.

$$L_{i+1}^d = 1 - 2 \times L_i^d, \quad L_i^d \in (-1, 1) \tag{40}$$

According to logical self-mapping function, the agents in BA are converted to [-1, 1], as Eq. (41), then, the initial agents can be obtained by transformation, as Eq. (42).

$$L_i^d = \frac{2(x_i^0 - a_i^d)}{b_i^d - a_i^d} - 1 \tag{41}$$

$$x_i^0 = \frac{(b_i^d - a_i^d) \times L_i^d + (b_i^d + a_i^d)}{2} \tag{42}$$

where b_i^d and a_i^d stand for the maximum and minimum, respectively.

To improve the diversity of pulse rate, the pulse rate updation is modified using the sine map as Eq. (43). From Fig.5, it can be seen that the sine map pulse rate $r_i(t)$ are within the range (0.5, 1) that exhibits better Chaos ergodicity.

$$r_{i+1}^d = \tau \times (r_i^d)^2 \times \sin(\pi r_i^d) \tag{43}$$

where τ stands for iteration parameter and is set as 2.3.

Finally, to enhance the convergence rapidity and precision, adaptive weighted disturbance coefficient, shown as Eq. (44), is applied to adjust the position of population in the iteration process.

$$\begin{cases} \omega(t) = \omega_{\max} \times \dfrac{(\omega_{\max} - \omega_{\min}) \times (T_{\max} - t)}{T_{\max}} \\ x_i(t) = \omega(t) \times x_i(t-1) + v_i(t-1) \end{cases} \tag{44}$$

where ω_{max} and ω_{min} denote the initial weighted coefficient and the final weighted coefficient, respectively. t and T_{max} are the current and the maximal iteration number, respectively.

3) VERIFICATION TEST OF IBA

Two standard test functions, including Rosenbrock and Schaffer F6 expressed as Eqs. (45) and (46), respectively, are used to investigate the effectiveness of IBA.

1) Rosenbrock

$$f_1 = 100(x_1^2 - x_2)^2 + (1 - x_1)^2, \quad -2.048 < x_1, x_2 < 2.048 \tag{45}$$

2) Schaffer F6

$$f_2 = \frac{\sin^2(\sqrt{x_1^2 + x_2^2}) - 0.5}{[1 + 0.001(x_1^2 + x_2^2)]^2}, \quad -100 < x_1, x_2 < 100 \tag{46}$$

In BA, the range of frequency $[f_{min}, f_{max}]$ is [0, 2], the maximum pulse emission r^0 and loudness A are set as 0.5 and 0.2, respectively, the coefficient parameter θ and pulse rate η are set as 0.95 and 0.05, respectively, and number of agents and maximum iteration are 30 and 100, respectively. The dimensions of Rosenbrock and Schaffer F6 are set as 2. The testing results are shown in Table 2 and Fig.6. It can be seen from Table 2 and Fig. 6 that IBA outperforms standard BA and PSO algorithms because IBA can jump out of local extremum easily for mutation and disturbance, and determine the global optimal values.

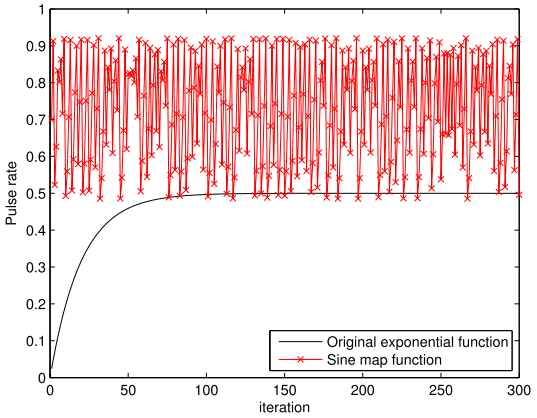

FIGURE 5. Pulse emission rate functions.

TABLE 2. Optimization results of different algorithms.

Function	Rosenbrock			Schaffer F6		
	best	worst	average	best	worst	average
BA	0.0052	0.1276	0.0557	-0.9783	-0.9218	-0.9476
IBA	0.0000	0.0097	0.0015	-0.9998	0.9658	0.9815
PSO	0.0001	0.0599	0.0096	-0.9895	0.9411	0.9583

4) IMPROVED MULTI-OBJECTIVE BAT ALGORITHM (IMOBA) FOR OPTIMIZATION OF EMS IN MG

As above description, two optimization objectives with a few constraints should be considered in this study, one is operation cost F_1, the other is pollution emission F_2, which is expressed as $min(F_1, F_2)$. Thus, the multi-objective

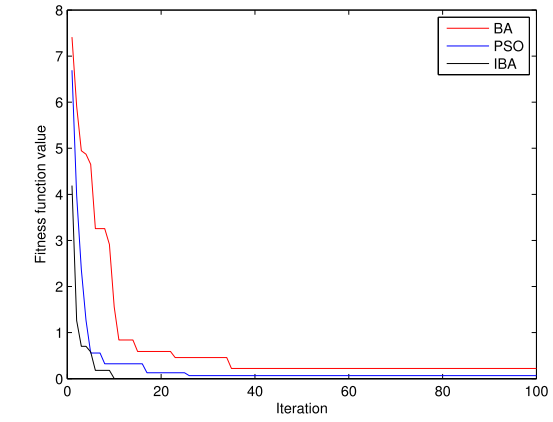

(a) Rosenbrock

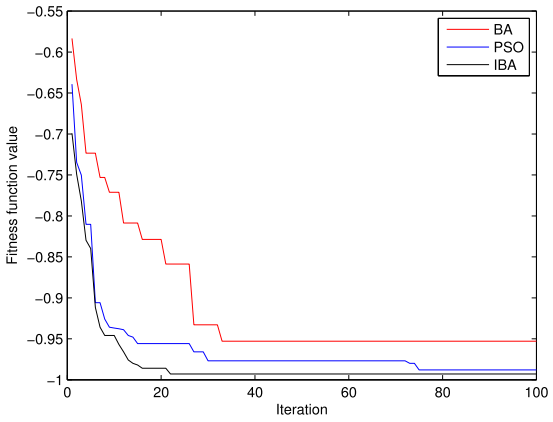

(b) Schaffer F6

FIGURE 6. Optimization curve of different test function.

optimization process of MG is to minimize the multi-objective functions under the constraints within the maximum iteration. The flowchart of IMOBA for multi-objective optimal dispatching of MG is shown in Algorithm 1.

Algorithm 1 IMOBA for Multi-Objective Optimal Dispatching for MG

Initialize the parameters in IBA, including dimension number, population number n, maximum iteration number $iter_{max}$ and so on, and generate the initial population by Chaos function Eq. (42).
for $i = 1 : n$ **do**
  Calculate the operational cost objective function and the pollutant emission objective function according to Eqs. (20) and (24), respectively, under corresponding technological constraints.
end for
Apply FST approach to determine the compromise solutions O^*according to Eqs. (32) and (33).
while $t < iter_{max}$ **do**
  for $i = 1 : n$ **do**
    Update the velocity $v_i(t)$, pulse frequency r_i and position $x_i(t)$ according to Eqs. (35), (43) and (44), respectively.
    Calculate corresponding operational cost objective function and the pollutant emission objective function according to Eqs. (20) and (24), respectively.
  end for
  Determine the compromise solutions O_{best} by Eqs. (32) and (33).
  if $O_{best} > O^*$ **then**
    $O^* = O_{best}$.
  else
    for $j = 1 : n$ **do**
      Generate new solution according to Eq. (37).
      if $A(t) > random$ **then**
        $A_i(t+1) = \theta \cdot A_i(t)$.
        $r_{i+1}^d = \tau \times (r_i^d)^2 \times \sin(\pi r_i^d)$.
      end if
    end for
  end if
  $t = t + 1$.
end while

IV. SIMULATION AND RESULTS

In this section, the proposed approach is employed to optimize the energy dispatching of the typical grid-connected MG, which consists of WT, ESS, PV, MT, FC, EMS, and upstream power grid, as shown in Fig. 4. Prior to applying the proposed approach to solve the multi-objective optimization, some input information should be determined in advance, which are presented as follows.

1) According to the WT of the FD23-50kW kind in the wind farm, the cut-in wind speed and cut-out wind speed are 2 m/s and 25 m/s, respectively, and the maximum power output of the WT are 50kW. The WPF results by CEEMDAN-IBA-GPR model under 90% confidence and the corresponding wind power are shown in Table 4. The power outputs of PV are set according to Ref. [6]. To evaluate and analyze the predicted performance of the proposed wind power forecasting model, three recently developed models, including support vector machines optimized by genetic algorithm combined with wavelet transform (WT-GA-SVM) [42], artificial neural networks combined with empirical mode decomposition (EMD-NN) [43] and BP neural network tuned by particle swarm optimization [44] combined with EEMD (EEMD-PSO-BPNN), are constructed and Diebold-Mariano (DM) tests [10], [45] are carried out to evaluate the proposed model based on statistical thinking. Expected values of forecasting results by the proposed model are used to compare with the forecasting results of the other models. The parameters in WT-GA-SVM, EMD-NN, and EEMD-PSO-BPNN are set according to the corresponding literatures. Table 3 indicates the testing results of DM. The results listed in the

TABLE 3. DM test results for the proposed wind power forecasting model and other three recently developed models.

Model	WT-GA-SVM	EEMD-PSO-BPNN	EMD-NN
Proposal	5.6655*	6.5226**	10.3723***

* **Note:**
*, **, *** denote 1%, 5% and 10% significance level, respectively.

table illustrates the proposed model is different from WT-GA-SVM at the 1% significance level, EEMD-PSO-BPNN at the 5% significance level, and EMD-NN at the 10% significance level.

2) Other parameters, such as loads of MG, bids of different DGs and so on, are set according to Refs. [6], [7], which are listed in Tables 5 ∼ 7.

Under different constraints, six main operation scenarios are designed and executed to investigate the multi-objective optimal power dispatching. The main ideas for selecting six operational scenarios are originated from the background knowledge of authors from the previous literatures [6], [7], [18] and practical considerations in power market bidding and distributed generators management. All the information is employed to optimize the power dispatching of grid-connected MG by considering the operation cost and the pollutant emission objectives under different economic and technological constraints. Optimal energy dispatching results reported in Tables 8 ∼ 14 are obtained using Matlab 2014a under Windows7 in personal computer with i5-2410U@2.40 GHz and 8GB RAM.

In the first scenario, all the DGs and ESS work under corresponding constraints, MG can exchange limited power with the upstream grid, and the aims of the first scenario are to investigate the overall optimization performance of IMOBA approach in the case of operational cost objective function. The optimal results are shown in the Table 8. As seen from the Table 8, the total operation cost for Scenario I is 1552.3 RMB while the pollutant emissions are 1475.8 kg. It can be also seen that the grid mainly sells electric power to MG in light-load period while the grid buys electric power from MG during peak-load period, which can effectively reduce the operational cost.

To illustrate the performance of IBA approach, the statistical indices of average and standard deviation, and operation time are utilized to compare with the conventional BA. The comparisons results are listed in Table 9 by considering operational cost in Scenario I. By comparing the statistical indices, the proposal IBA algorithm has better statistical indices of average and standard deviations, although it needs more operational time, which means it is efficient in solving the energy optimal dispatching of EEMS.

In the second scenario, the optimal energy management is obtained by the IMOBA according to the pollutant emission objective function, assumed that the renewable energy PV and WT can supply their maximum available capacity power while others operate under the same constraints in scenario I. The optimal results are shown in the Table 10. The pollutant emission in Scenario II is 838.1 kg while the total operation cost is 2859 RMB.

Remark: During the peak-load periods, the bids of grid power are higher than the energy price of DGs, while the electrical market bids are lower during light-load period. No matter during light-load or peak-load period,

TABLE 4. Wind power forecasting value and output of PV.

Hour	Forecasting interval [Min(kW)	Max(kW)]	Output of PV (kW)	Hour	Forecasting interval [Min(kW)	Max(kW)]	Output of PV (kW)
1	19.4324	22.3214	0	13	17.5008	19.2279	13.23
2	15.4325	17.6522	0	14	18.7842	20.9861	14.28
3	11.1184	14.2212	0	15	16.6335	18.3749	12.22
4	10.2318	13.6437	0	16	19.3288	22.3874	8.61
5	10.5614	14.2495	0	17	19.7876	21.3754	5.32
6	11.1282	14.5435	0	18	20.1988	23.6183	0.21
7	10.8349	13.1541	0.27	19	19.274	22.3462	0
8	10.6759	13.3665	0.77	20	15.8796	17.8739	0
9	11.9413	14.9015	2.89	21	17.7665	20.8331	0
10	14.7142	17.7718	8.98	22	22.5449	25.3117	0
11	15.8991	18.7872	11.34	23	27.6914	30.0821	0
12	16.437	18.2163	12.61	24	26.5781	29.1182	0

TABLE 5. Load demands of micro-grid (kW).

Hour	1h	2h	3h	4h	5h	6h	7h	8h	9h	10h	11h	12h
Power	68	65	65	70	73	78	88	95	107	109	113	110
Hour	13h	14h	15h	16h	17h	18h	19h	20h	21h	22h	23h	24h
Power	108	112	117	113	117	121	127	117	104	93	86	71

TABLE 6. Bids of DGs, battery and grid electricity in RMB/kW.

Hour	MT	FC	PV	WT	Battery	Grid	Hour	MT	FC	PV	WT	Battery	Grid
1	0.6373	0.9888	0	0.1626	0.923	0.266	13	0.6853	1.0128	0.5126	1.0608	1.3102	1.665
2	0.6373	0.9888	0	0.1316	0.923	0.209	14	0.6853	1.0128	0.5064	1.0453	1.2389	4.429
3	0.6435	0.995	0	0.1007	0.9826	0.155	15	0.6853	1.0128	0.5002	1.0221	1.1909	2.215
4	0.6435	0.9989	0	0.0852	1.0422	0.137	16	0.6969	1.0182	0.494	0.8827	1.1615	2.160
5	0.6489	0.995	0	0.3949	1.1019	0.137	17	0.7031	1.0306	0.5056	0.8518	1.1793	0.666
6	0.6489	1.0004	0	0.6582	1.1615	0.225	18	0.7085	1.0306	0.5126	0.7201	1.1615	0.457
7	0.6551	1.0004	0	0.7046	1.2211	0.266	19	0.7031	1.0361	0	0.7046	1.1321	0.387
8	0.6613	1.0066	0.5002	0.8518	1.2451	0.418	20	0.6853	1.0306	0	0.6427	1.1321	0.472
9	0.6675	1.0128	0.5064	1.0841	1.2869	1.665	21	0.6675	1.0182	0	0.2555	1.1081	1.402
10	0.6675	1.0182	0.5126	1.1073	1.2986	4.429	22	0.6551	1.0128	0	0.1936	1.0515	0.596
11	0.6907	1.0244	0.518	1.1615	1.3404	4.429	23	0.6489	1.0066	0	0.1626	1.0422	0.333
12	0.6969	1.0182	0.5242	1.2002	1.3698	4.429	24	0.6435	0.995	0	0.1316	0.9826	0.287

TABLE 7. Installed capacity of DGs and emission factors.

Type	Min power (kW)	Max power (kW)	Start-up/shutdown cost (RMB/kW)	Start-up/shutdown emission (kg/MW)	NO_x (kg/MW)	CO_2 (kg/MW)	SO_2 (kg/MW)
MT	10	50	0.8285	0.9	0.2	724	0.0036
FC	5	50	1.0686	0.52	0.0136	489	0.0027
Grid	-60	60	-	-	2.295	922	3.583
PV	0	30	-	-	-	-	-
WT	0	50	-	-	-	-	-
Battery	-50	50	-	-	-	-	-

TABLE 8. Optimal dispatching of MG for scenario I (kW) (Cost = 1552.3 RMB, Emission = 1475.8kg).

Hour	MT	FC	PV	WT	Battery	Grid	Hour	MT	FC	PV	WT	Battery	Grid
1	23.24	17.39	0	21.39	-47.81	53.78	13	48.1	36.2	10.65	18.68	-13.63	8
2	11.34	12.14	0	15.74	-33.67	59.46	14	44.5	20.84	9.7	19.11	42.01	-24.16
3	11.61	16.37	0	12.94	11.44	12.65	15	48.87	39.09	8.12	18.35	-39.59	42.15
4	47.51	30.99	0	11.21	-49.92	30.21	16	36.14	28.96	4.95	19.36	38.06	-14.46
5	39.57	11.34	0	13.75	-40.59	48.93	17	26.11	26.97	1.1	20.28	-8.75	51.29
6	32.47	6.49	0	13.59	-19.86	45.31	18	46.92	31.41	0.1	22.82	-20.69	40.43
7	23.75	17.91	0	11.02	-8.86	44.18	19	27.83	29.24	0.1	22.18	-10.60	58.25
8	25.06	14.45	0.1	11.95	-16.56	60	20	33.83	42.59	0	17.05	-12.53	36.06
9	48.6	39.78	0.59	14.61	-12.74	16.16	21	47.1	43.99	0	20.2	-3.93	-3.36
10	37.44	47.81	1.98	15.66	-18.8	24.92	22	47.85	27.5	0	22.6	-19.88	14.93
11	36.99	47.43	7.75	16.24	37.98	-33.38	23	47.13	15.72	0	28.31	10.15	-15.32
12	38.18	46.86	9.8	17.17	12.03	-14.04	24	23.45	26.33	0	27.93	-35.59	28.88

* **Note:**

[1)] Positive and negative power for grid represent the selling power to MG and the buying power from MG, respectively.
[2)] Positive and negative power for battery represent discharging and charging, respectively.
[3)] The corresponding definitions in the tables at the back are the same meaning.

TABLE 9. Optimal results of Scenario I with respect to cost objective for 30 trials.

Optimization algorithm	Best solution (RMB)	Worst solution (RMB)	Average solution (RMB)	Average time (s)	Stand deviation (RMB)
PSO	1568.81	1654.33	1592.77	14.69	14.15
MOBA	1610.13	1692.37	1661.29	13.73	18.58
IMOBA	1552.37	1602.91	1570.64	14.12	10.42

the pollutant emissions of the utility grid are higher. Thus, minimum operating costs or minimum pollutant emissions in MG can be obtained by exchanging power with the utility grid. Over the operational period of Scenario I, the total power that MG exchanges with the power grid system is 577.9 kW, and the total power in the operational period of Scenario II is −16.98 kW, the capacity of exchanging power with the power grid system can effectively reduce the operation cost and managers are more inclined to buy power from the grid system in the terms of cost, however, the high pollutant

TABLE 10. Optimal dispatching of MG for scenario II (kW) (Cost = 2859 RMB, Emission = 838.1kg).

Hour	MT	FC	PV	WT	Battery	Grid	Hour	MT	FC	PV	WT	Battery	Grid
1	21.34	11.34	0	22.32	24.19	-11.19	13	42.37	27.57	10.65	19.23	6.09	2.09
2	12.7	18.51	0	17.65	18.65	-2.51	14	22.62	37.33	9.7	20.99	9.64	11.72
3	21.8	33.92	0	14.22	-18.32	13.38	15	39.1	39.98	8.12	18.37	-22.92	34.35
4	18.49	30.5	0	13.64	34.37	-27	16	39.43	9.36	4.95	22.39	41.32	-4.45
5	34.42	27.21	0	14.25	24.81	-27.69	17	33.98	32.78	1.1	21.38	-6.26	34.02
6	25.69	8.04	0	14.54	31.83	-2.1	18	37.09	28.18	0.1	23.62	47.06	-15.05
7	21.2	39.53	0	13.15	28.31	-14.19	19	26.56	23.54	0.1	22.35	27.83	26.62
8	14.42	35.03	0.1	13.37	38.57	-6.49	20	38.76	48.78	0	17.87	-17.92	29.51
9	47.3	45.03	0.59	14.9	-17.73	16.91	21	22.48	43.77	0	20.83	27.08	-10.16
10	35.8	17.14	1.98	17.77	45.16	-8.85	22	28.78	38.17	0	25.31	23.72	-22.98
11	39.72	42.43	7.75	18.79	-21.86	26.17	23	20.63	13.6	0	30.08	33.5	-11.81
12	32.3	26.63	9.8	18.22	33.8	-10.75	24	12.66	46.34	0	29.12	19.41	-36.53

emission of the power grid system prevents the behavior. It can also be obtained that the batteries almost charge and the MG buys power from the grid system when the electrical power price of grid is lowest, while the batteries discharge and the MG sells power to the grid system in the hours of high-power price, thus, this contribute to low operation cost of MG in Scenario I and low pollutant emission of MG in Scenario II.

In the third scenario, assumed that MG can buy and sell unlimited power energy with the upstream grid and other DGs operate under their respective constraints. The IMOBA algorithm is firstly employed to minimize both operational cost and pollutant emission function objectives based on 24-POF-per-day dispatching scheme. In the scenario III, optimal hourly set points of energy management over 24h ahead are considered to determine one optimal solution or one POF per day, in the other words, 24 primary objectives corresponding to 24h a day are aggregated to yield the final multi-objective solution. The POF solutions obtained by IMOBA, MOBA and PSO approaches are shown in Fig. 7, and it can be obviously observed from the figure that IMOBA approach can solve the power dispatching problem of grid-connected MG successfully while maintains smallest multi-objective values in finding optimal solutions. The compromise solutions for scenarios III by IMOBA are determined from the obtained POFs by FST theory, which are shown in the Table 11. The pollutant emission in Scenario III is 917 kg while the total operation cost is 2477.2 RMB.

In the fourth scenario, to enhance the decision flexibility for operators, one-POF-per-hour optimization scheme is designed in scenario IV with the same constraints in scenario III. It is assumed that the initial state of ESS is infinitive. The POF solutions for the typical hours are shown in Fig. 8 and the compromise solutions are determined from the obtained POFs by FST method, which are shown in the Table 12. As seen from the Table 12, the total aggregated compromise results of operational cost and net pollutant emission for a day are 1867.9 RMB and 624.9 kg, respectively. From the figure, it is obvious that different POFs are yielded at different hour of the day for different power output of DGs, market price, and load demands.

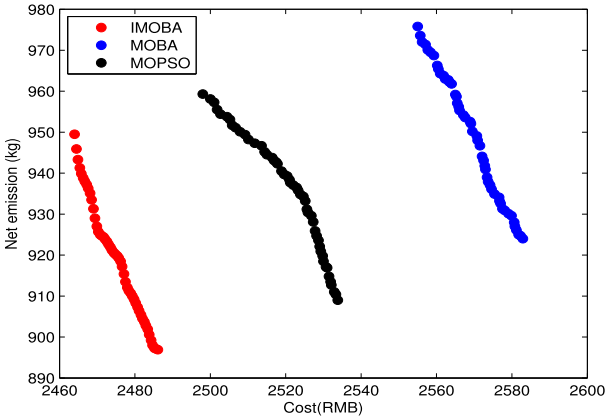

FIGURE 7. POF for Scenario III obtained by different approaches.

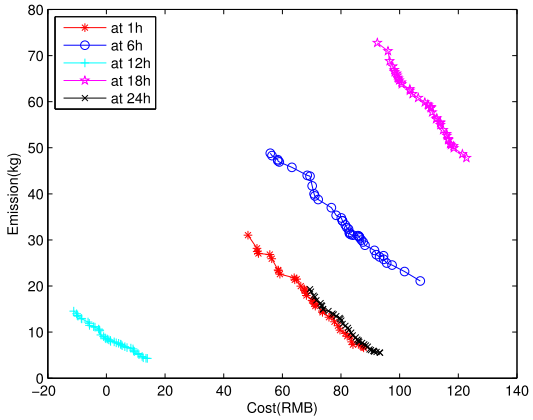

FIGURE 8. POF for Scenario IV obtained by IMOBA for some hours.

Remark: As seen from the Tables 8, 10 and 11, the total operation cost for Scenarios I, II, III are 1552.3 RMB, 2859RMB, and 2477.2 RMB, respectively, the total pollutant emissions are 1475.8 kg, 838.1 kg, and 917 kg, respectively. The total operational cost for the scenario I is smallest because only operational cost objective is considered, meanwhile, the total pollutant emission for the Scenario II is smallest because only pollutant emission objective is considered. Compared with the optimal results of the first scenario, the total operational cost of scenario III increases by

TABLE 11. Optimal dispatching of MG for scenario III (kW) (Cost = 2477.2 RMB, Emission = 917 kg).

Hour	MT	FC	PV	WT	Battery	Grid	Hour	MT	FC	PV	WT	Battery	Grid
1	43.47	12.34	0	20.02	-15.6	7.77	13	45.14	27.82	10.65	17.53	27.82	-20.96
2	19.97	20.56	0	17.62	12.4	-5.54	14	24.38	43.18	9.7	19.74	10.58	4.42
3	33.85	30.98	0	12.37	4.54	-16.74	15	25.1	37.46	8.12	17.18	44.94	-15.81
4	41.1	26.17	0	10.53	43.39	-51.19	16	43.99	39.9	4.95	20.24	37.27	-33.36
5	28.74	34.19	0	13.26	-40.68	37.49	17	25	40.93	1.1	21.08	49.9	-21.01
6	41.42	46.62	0	13.06	-4.58	-18.52	18	17.8	15.66	0.1	21.67	34.72	31.05
7	41.74	17.77	0	13.14	48.6	-33.25	19	31.46	47.53	0.1	22.08	-11.77	37.6
8	31.45	45.25	0.1	11.31	-2.15	9.04	20	33.63	41.56	0	16.4	48.58	-23.17
9	46.3	34.87	0.59	13.23	35.4	-23.39	21	27.65	15.14	0	18.33	19.82	23.06
10	36.84	39.09	1.98	16.09	-10.6	25.6	22	45.01	35.1	0	23.27	-34.57	24.19
11	27.83	44.75	7.75	16.89	25.39	-9.61	23	31.77	20.49	0	29.3	-44.33	48.77
12	22.39	46.92	9.8	16.73	45.29	-31.13	24	12.18	30.42	0	28.23	-26.3	26.46

TABLE 12. Optimal dispatching of MG for scenario IV (kW) (Cost = 1867.9 RMB, Emission = 624.9 kg).

Hour	MT	FC	PV	WT	Battery	Grid	Cost (RMB)	Emission (kg)
1	23.68	12.27	0	21.9	16.06	-5.92	67.59	17.67
2	16.9	7.96	0	16.67	23.09	0.39	67.56	16.49
3	19.71	34.95	0	13.73	-21.62	18.23	29.63	48.28
4	13.46	14.45	0	12.6	19.55	9.95	68.83	26.04
5	25.66	10.7	0	13.02	12.49	11.13	66.1	34.14
6	17.6	12.91	0	14.54	20.71	12.25	85.16	30.42
7	15.99	5.81	0	12.83	23.77	29.61	86.15	41.89
8	12.93	15.59	0.1	13.17	24.33	28.88	104.8	43.78
9	47.3	49.96	0.59	14.29	38.55	-43.68	125.44	18.15
10	43.45	46.7	1.98	16.77	46.59	-46.5	6.25	11.17
11	47.29	48.97	7.75	18.3	41.64	-50.96	-7.97	10.92
12	49.29	39.08	9.8	17.04	45.37	-50.58	-29.35	6.75
13	47.9	46.12	10.65	18.71	39.93	-55.31	117.77	5.92
14	49.83	48	9.7	19.77	43.19	-58.48	-41.77	5.29
15	49.71	42.8	8.12	17.46	49.84	-50.94	104.53	9.67
16	40.23	43.32	4.95	22.12	49.9	-47.51	108.03	6.23
17	38.45	21.94	1.1	20.85	11.33	17.33	124.89	57.54
18	44.65	16.24	0.1	22.78	25.75	5.49	134.46	50.93
19	18.85	31.93	0.1	19.51	22.91	25.7	135.07	58.91
20	35.01	12.23	0	17.87	26.21	25.68	121.24	55.16
21	44.5	33.73	0	18.19	41.22	-33.65	116.19	17.51
22	25.61	6.49	0	25.26	28.99	6.65	95.28	27.89
23	28.56	21.28	0	29.48	20.32	-13.65	92.86	18.43
24	49.38	8.41	0	28.67	21.27	-36.73	89.16	5.79

894.9 RMB and the total net pollutant emission decreases by 558.8 kg. Compared with that of the second scenario, the total operational cost of scenario III decreases by 411.8 RMB while the total net pollutant emission increases by 78.9 kg. The reasons of which are that the compromise solutions are obtained based on the multi-objective optimal perspective. Compared with Scenario III, both the optimal operational cost and pollutant emission for Scenario IV are decreases by 579.3 RMB and 292.1 kg, respectively. The one-POF-per-hour scheme not only provides flexibility for operators but also obtains better energy dispatching results. From Table 12, almost all the batteries in ESS system, apart from 3h, are in the state of discharging, which should be considered in the actual application.

In the previous $1^{st} \sim 4^{st}$ scenarios, all the DGs operates in *ON* state. It is assumed that all the DGs in the fifth scenario can operate in *ON* or *OFF* states and the exchanging power between MG and the grid is unrestricted. The other assumptions are the same as that in the fourth scenario. The compromise optimization solutions obtained by two-step methodology are shown in the Table 13. During low market price periods in 1h $\sim$ 8h and 17h $\sim$ 24h, either MT or FC is in the *OFF* states and the upstream grid provides power for MG, while grid purchases power from MG and all the DGs are in the *ON* states during high market price periods in 9h $\sim$ 16h. Compared with the fourth scenario, the total net pollutant emission increases 217.1 kg while the total operational cost decreases 421.2 RMB. In addition, the battery is always on the state of discharging in the whole day. According to the table, wind power and photovoltaic energy are preferred all the time.

In the sixth scenario, all the DGs are in the state of *ON*, the limited capacity and technique constraints of batteries in ESS are considered. It is assumed that 20% and 100% of the battery capacity are considered as the lower and upper limits on the state of charge (SOC), respectively. One-POF-one-hour optimization strategy is also adopted in this scenario. The other characteristic parameters of batteries

TABLE 13. Optimal dispatching of MG for scenario V (kW) (Cost = 1580.7 RMB, Emission =842.1 kg).

Hour	Operational state						Output power (kW)						Cost	Emission
	MT	FC	PV	WT	Battery	Grid	MT	FC	PV	WT	Battery	Grid	(RMB)	(kg)
1	0	1	1	1	1	1	0	5.49	0	20.88	19.98	21.65	54.25	22.77
2	0	1	1	1	1	1	0	5.63	0	16.54	19.35	23.48	50.43	24.54
3	0	1	1	1	1	1	0	5.11	0	12.67	18.83	28.39	53.11	28.84
4	1	0	1	1	1	1	10.41	0	0	11.94	10.26	37.39	43.83	42.25
5	0	1	1	1	1	1	0	6.21	0	12.41	15.39	38.99	55.94	39.22
6	1	0	1	1	1	1	10.79	0	0	12.84	10.58	43.79	58.92	48.47
7	0	1	1	1	1	1	0	6.75	0	11.99	13.38	55.88	67.72	55.16
8	1	0	1	1	1	1	13.14	0	0.1	12.02	7.67	62.06	75.79	67.12
9	1	1	1	1	1	1	49.3	47.57	0.59	13.42	37.88	-41.77	175.51	20.23
10	1	1	1	1	1	1	47.27	48.8	1.98	16.24	49.87	-55.16	-20.64	6.91
11	1	1	1	1	1	1	47.6	48.7	7.75	17.34	49.74	-58.13	-24.52	4.35
12	1	1	1	1	1	1	46.42	48.75	9.8	17.33	48.84	-61.14	-37.26	0.73
13	1	1	1	1	1	1	49.38	49.31	10.65	18.36	46.81	-66.5	117.93	-1.84
14	1	1	1	1	1	1	47.72	49.09	9.7	19.89	49.72	-64.12	-54.07	-0.93
15	1	1	1	1	1	1	49.65	49.8	8.12	17.5	43.68	-51.75	99.77	12.29
16	1	1	1	1	1	1	48.41	47.73	4.95	20.86	46.95	-55.9	146.19	6.55
17	1	0	1	1	1	1	49.45	0	1.1	20.58	0.81	39.06	132.96	72.1
18	0	1	1	1	1	1	0	5.33	0.1	21.91	15.85	71.8	97.02	69.24
19	0	1	1	1	1	1	0	6.7	0.1	20.81	16.15	75.24	88.06	73.09
20	0	1	1	1	1	1	0	6.56	0	16.88	17.7	75.86	99.67	73.61
21	1	0	1	1	1	1	49.72	0	0	19.3	24.45	10.53	150.18	45.82
22	1	0	1	1	1	1	49.66	0	0	23.93	2.17	17.24	63.6	51.96
23	1	0	1	1	1	1	11.68	0	0	28.89	8.69	36.73	58.53	42.56
24	0	0	1	1	1	1	0	0	0	27.85	3.2	39.95	27.79	37.07

TABLE 14. Optimal dispatching of MG for scenario VI (kW) (Cost = 1482.6 RMB, Emission =1108.2 kg).

Hour	MT	FC	PV	WT	Battery	Grid	Cost (RMB)	Emission (kg)
1	11.01	38.79	0	20.88	-27.67	24.99	26.2	50.13
2	10.26	38.46	0	16.54	-27.43	27.17	22.59	51.45
3	10.35	40.83	0	12.67	-26.92	28.07	21.89	53.51
4	10.28	40.72	0	11.94	-23.66	30.72	25.29	55.86
5	10.07	41.73	0	12.41	-25.48	34.27	26.01	59.5
6	12.34	34.73	0	12.84	-25.91	44	25.88	66.75
7	11.38	39.38	0	11.99	-13.53	38.78	53.52	63.48
8	49.25	20.23	0.1	12.02	-1.85	15.25	80.36	59.71
9	49.61	49.73	0.59	13.42	12.39	-18.74	114.62	42.86
10	49.89	49.66	1.98	16.24	27.89	-36.66	20.06	26.4
11	49.08	49.87	7.75	17.34	26.08	-37.11	22.47	25.49
12	49.59	49.96	9.8	17.33	27.17	-43.85	-1.86	19.66
13	49.93	49.34	10.65	18.36	17.75	-38.03	106.56	25
14	49.61	49.9	9.7	19.89	23.51	-40.61	1.25	22.65
15	49.97	49.67	8.12	17.5	21.71	-29.97	105.98	32.67
16	49.66	49.24	4.95	20.86	13.28	-24.98	101.36	36.86
17	49.82	22.73	1.1	20.58	-3.22	19.98	101.21	65.74
18	49.32	20.91	0.1	21.91	11.74	11.02	116.77	56.17
19	10.8	38.15	0.1	20.81	27.06	22.08	137.47	46.96
20	49.05	20.22	0	16.88	23.96	6.88	128.9	51.8
21	47.68	49.38	0	19.3	-1.47	-10.89	92.67	48.57
22	49.9	21.48	0	23.93	-12.45	10.14	60.81	56.05
23	15.94	35.79	0	28.89	-15.48	20.86	49.23	48.4
24	49.93	21.51	0	27.85	-23.87	-4.43	43.32	42.57

are set according to Ref. [18]. The hourly battery SOC is shown in Fig. 9 and the compromise optimization results are listed in the Table 14. Seen from the figure, the red lines represent the limits on the battery SOC, the battery discharging is preferred from 9h to 21h which are the high load hours and high market price period, and the battery packs are selected for charging action at the low load hours from 1h to 8h and 22h to 24h. Compared with the fifth scenario, both operational cost and pollutant emission increase, which is caused by technical constraints of the batteries.

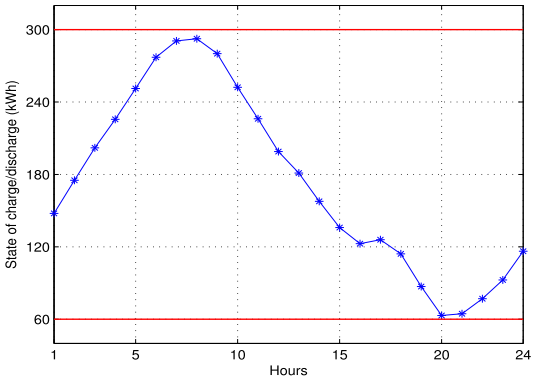

FIGURE 9. Hourly state of battery charge/discharge.

Compared with Tables 8 $\sim$ 11, the optimization power dispatching of each hour in Tables 12 $\sim$ 14 can provide more flexibility for decision makers to determine optimal energy set points. As for wind power and photovoltaic power with inexpensive and free emission characteristics, the operators intend to make use of the maximum available power of the renewable energy in the most time of all scenarios.

V. CONCLUSION

In this study, a new EEMS considering wind power probability for energy optimal dispatching of grid-connected MG is proposed by minimizing operational economic cost and net pollutant emission objectives simultaneously. To address the optimization dispatching problems, a two-step solution method integrating an improved multi-objective bat algorithm with fuzzy set theory is developed to automatically generate optimal compromise solutions for decision makers. The results of six operational scenarios of MG show that EEMS can effectively schedule the generation power of DGs, ESS and the exchanging power between the upstream grid and MG according to economic cost and pollutant emission objectives.

Optimal dispatching of isolated or grid-connected MG considering economic cost, net pollutant emission, and operational security objectives will be research focus in the future work. It is significant to study optimal dispatching of a grid-connected MG containing MT, WT, PV, FC, ESS and electric vehicle battery swapping station under demand responses conditions.

REFERENCES

[1] M. Mansour-Lakouraj and M. Shahabi, "Comprehensive analysis of risk-based energy management for dependent micro-grid under normal and emergency operations," *Energy*, vol. 171, pp. 928–943, Mar. 2019, doi: 10.1016/j.energy.2019.01.055.

[2] S. A. Alavi, A. Ahmadian, and M. Aliakbar-Golkar, "Optimal probabilistic energy management in a typical micro-grid based-on robust optimization and point estimate method," *Energy Convers. Manage.*, vol. 95, pp. 314–325, May 2015, doi: 10.1016/j.enconman.2015.02.042.

[3] M. H. Alham, M. Elshahed, D. K. Ibrahim, and E. E. D. A. El Zahab, "A dynamic economic emission dispatch considering wind power uncertainty incorporating energy storage system and demand side management," *Renew. Energy*, vol. 96, pp. 800–811, Oct. 2016, doi: 10.1016/j.renene.2016.05.012.

[4] Y.-Y. Hong and J.-K. Lin, "Interactive multi-objective active power scheduling considering uncertain renewable energies using adaptive chaos clonal evolutionary programming," *Energy*, vol. 53, pp. 212–220, May 2013, doi: 10.1016/j.energy.2013.02.070.

[5] S. Abedi, A. Alimardani, G. B. Gharehpetian, G. H. Riahy, and S. H. Hosseinian, "A comprehensive method for optimal power management and design of hybrid RES-based autonomous energy systems," *Renew. Sustain. Energy Rev.*, vol. 16, no. 3, pp. 1577–1587, Apr. 2012, doi: 10.1016/j.rser.2011.11.030.

[6] J. Sarshar, S. S. Moosapour, and M. Joorabian, "Multi-objective energy management of a micro-grid considering uncertainty in wind power forecasting," *Energy*, vol. 139, pp. 680–693, Nov. 2017, doi: 10.1016/j.energy.2017.07.138.

[7] M. Motevasel and A. R. Seifi, "Expert energy management of a micro-grid considering wind energy uncertainty," *Energy Convers. Manage.*, vol. 83, pp. 58–72, Jul. 2014, doi: 10.1016/j.enconman.2014.03.022.

[8] S. Sun, L. Wei, and J. Xu, "A new wind power forecasting modeling strategy using two-stage decomposition, feature selection and DAWNN," *Energies*, vol. 12, no. 3, pp. 12334-1–12334-24, Feb. 2019, doi: 10.3390/en12030334.

[9] S. Sun, J. Fu, F. Zhu, and D. Du, "A hybrid structure of an extreme learning machine combined with feature selection, signal decomposition and parameter optimization for short-term wind speed forecasting," *Trans. Inst. Meas. Control*, vol. 42, no. 1, pp. 3–21, May 2018, doi: 10.1177/0142331218771141.

[10] J. Wang, J. Heng, L. Xiao, and C. Wang, "Research and application of a combined model based on multi-objective optimization for multi-step ahead wind speed forecasting," *Energy*, vol. 125, pp. 591–613, Apr. 2017, doi: 10.1016/j.energy.2017.02.150.

[11] H. Yin, Z. Dong, Y. Chen, J. Ge, L. L. Lai, A. Vaccaro, and A. Meng, "An effective secondary decomposition approach for wind power forecasting using extreme learning machine trained by crisscross optimization," *Energy Convers. Manage.*, vol. 150, pp. 108–121, Oct. 2017, doi: 10.1016/j.enconman.2017.08.014.

[12] E. Xydas, M. Qadrdan, C. Marmaras, L. Cipcigan, N. Jenkins, and H. Ameli, "Probabilistic wind power forecasting and its application in the scheduling of gas-fired generators," *Appl. Energy*, vol. 192, pp. 382–394, Apr. 2017, doi: 10.1016/j.apenergy.2016.10.019.

[13] Y. Wang, Q. Hu, D. Meng, and P. Zhu, "Deterministic and probabilistic wind power forecasting using a variational Bayesian-based adaptive robust multi-kernel regression model," *Appl. Energy*, vol. 208, pp. 1097–1112, Dec. 2017, doi: 10.1016/j.apenergy.2017.09.043.

[14] S. M. Moghaddas-Tafreshi, S. Mohseni, M. E. Karami, and S. Kelly, "Optimal energy management of a grid-connected multiple energy carrier micro-grid," *Appl. Thermal Eng.*, vol. 152, pp. 796–806, Apr. 2019, doi: 10.1016/j.applthermaleng.2019.02.113.

[15] X. Jin, Y. Mu, H. Jia, J. Wu, T. Jiang, and X. Yu, "Dynamic economic dispatch of a hybrid energy microgrid considering building based virtual energy storage system," *Appl. Energy*, vol. 194, pp. 386–398, May 2017, doi: 10.1016/j.apenergy.2016.07.080.

[16] S. Mohseni, A. C. Brent, and D. Burmester, "A demand response-centred approach to the long-term equipment capacity planning of grid-independent micro-grids optimized by the moth-flame optimization algorithm," *Energy Convers. Manage.*, vol. 200, Nov. 2019, Art. no. 112105, doi: 10.1016/j.enconman.2019.112105.

[17] K. Roy, K. K. Mandal, and A. C. Mandal, "Ant-lion optimizer algorithm and recurrent neural network for energy management of micro grid connected system," *Energy*, vol. 167, pp. 402–416, Jan. 2019, doi: 10.1016/j.energy.2018.10.153.

[18] A. Deihimi, B. K. Zahed, and R. Iravani, "An interactive operation management of a micro-grid with multiple distributed generations using multi-objective uniform water cycle algorithm," *Energy*, vol. 106, pp. 482–509, Jul. 2016, doi: 10.1016/j.energy.2016.03.048.

[19] M. Azaza and F. Wallin, "Multi objective particle swarm optimization of hybrid micro-grid system: A case study in sweden," *Energy*, vol. 123, pp. 108–118, Mar. 2017, doi: 10.1016/j.energy.2017.01.149.

[20] X. Liang, X. He, and T. Huang, "Distributed neuro-dynamic optimization for multi-objective power management problem in micro-grid," *Neurocomputing*, vol. 362, pp. 51–59, Oct. 2019, doi: 10.1016/j.neucom.2019.05.096.

[21] T. Lv, Q. Ai, and Y. Zhao, "A bi-level multi-objective optimal operation of grid-connected microgrids," *Electr. Power Syst. Res.*, vol. 131, pp. 60–70, Feb. 2016, doi: 10.1016/j.epsr.2015.09.018.

[22] Y. Li, Z. Yang, D. Zhao, H. Lei, B. Cui, and S. Li, "Incorporating energy storage and user experience in isolated microgrid dispatch using a multi-objective model," *IET Renew. Power Gener.*, vol. 13, no. 6, pp. 973–981, Apr. 2019.

[23] W. Jun, L. Yuyan, T. Lingyu, and G. Peng, "A new weighted CEEMDAN-based prediction model: An experimental investigation of decomposition and non-decomposition approaches," *Knowl.-Based Syst.*, vol. 160, pp. 188–199, Nov. 2018, doi: 10.1016/j.knosys.2018.06.033.

[24] L. Wang and Y. Shao, "Fault feature extraction of rotating machinery using a reweighted complete ensemble empirical mode decomposition with adaptive noise and demodulation analysis," *Mech. Syst. Signal Process.*, vol. 138, Apr. 2020, Art. no. 106545.

[25] T. Peng, J. Zhou, C. Zhang, and Y. Zheng, "Multi-step ahead wind speed forecasting using a hybrid model based on two-stage decomposition technique and AdaBoost-extreme learning machine," *Energy Convers. Manage.*, vol. 153, pp. 589–602, Dec. 2017, doi: 10.1016/j.enconman.2017.10.021.

[26] X. Wen, Q. Feng, R. C. Deo, M. Wu, Z. Yin, L. Yang, and V. P. Singh, "Two-phase extreme learning machines integrated with the complete ensemble empirical mode decomposition with adaptive noise algorithm for multi-scale runoff prediction problems," *J. Hydrol.*, vol. 570, pp. 167–184, Mar. 2019, doi: 10.1016/j.jhydrol.2018.12.060.

[27] C. Zhang, H. Wei, J. Zhao, T. Liu, T. Zhu, and K. Zhang, "Short-term wind speed forecasting using empirical mode decomposition and feature selection," *Renew. Energy*, vol. 96, pp. 727–737, Oct. 2016, doi: 10.1016/j.renene.2016.05.023.

[28] W. Sun and Y. Wang, "Short-term wind speed forecasting based on fast ensemble empirical mode decomposition, phase space reconstruction, sample entropy and improved back-propagation neural network," *Energy Convers. Manage.*, vol. 157, pp. 1–12, Feb. 2018, doi: 10.1016/j.enconman.2017.11.067.

[29] J. Hu and J. Wang, "Short-term wind speed prediction using empirical wavelet transform and Gaussian process regression," *Energy*, vol. 93, pp. 1456–1466, Dec. 2015, doi: 10.1016/j.energy.2015.10.041.

[30] V. Hoolohan, A. S. Tomlin, and T. Cockerill, "Improved near surface wind speed predictions using Gaussian process regression combined with numerical weather predictions and observed meteorological data," *Renew. Energy*, vol. 126, pp. 1043–1054, Oct. 2018, doi: 10.1016/j.renene.2018.04.019.

[31] J. Hu, J. Wang, and K. Ma, "A hybrid technique for short-term wind speed prediction," *Energy*, vol. 81, pp. 563–574, Mar. 2015, doi: 10.1016/j.energy.2014.12.074.

[32] A. Meng, J. Ge, H. Yin, and S. Chen, "Wind speed forecasting based on wavelet packet decomposition and artificial neural networks trained by crisscross optimization algorithm," *Energy Convers. Manage.*, vol. 114, pp. 75–88, Apr. 2016, doi: 10.1016/j.enconman.2016.02.013.

[33] J. Naik, P. K. Dash, and S. Dhar, "A multi-objective wind speed and wind power prediction interval forecasting using variational modes decomposition based multi-kernel robust ridge regression," *Renew. Energy*, vol. 136, pp. 701–731, Jun. 2019, doi: 10.1016/j.renene.2019.01.006.

[34] M. Farina and P. Amato, "A fuzzy definition of 'optimality' for many-criteria optimization problems," *IEEE Trans. Syst., Man, Cybern. A, Syst., Humans*, vol. 34, no. 3, pp. 315–326, May 2004, doi: 10.1109/TSMCA.2004.824873.

[35] X.-S. Yang, "Bat algorithm for multi-objective optimization," *Int. J. Bio-Inspired Comput.*, vol. 3, no. 5, pp. 267–274, Sep. 2011, doi: 10.1504/IJBIC. 2011.042259.

[36] T. Tharakeshwar, K. Seetharamu, and P. Durga, "Multi-objective optimization using bat algorithm for shell and tube heat exchangers," *Appl. Therm. Eng.*, vol. 110, no. 5, pp. 1029–1038, Jan. 2017, doi: 10.1016/.j.applthermaleng.2016.09.031.

[37] M. Zineddine, "Optimizing security and quality of service in a real-time operating system using multi-objective bat algorithm," *Future Gener. Comput. Syst.*, vol. 87, pp. 102–114, Oct. 2018, doi: 10.1016/j.future.2018.02.043.

[38] N. Yang and M. Le, "Optimal design of passive power filters based on multi-objective bat algorithm and Pareto front," *Appl. Soft Comput.*, vol. 35, pp. 257–266, Oct. 2015, doi: 10.1016/.j.asoc.2015.05.042.

[39] P. Jiang, R. Li, and H. Li, "Multi-objective algorithm for the design of prediction intervals for wind power forecasting model," *Appl. Math. Model.*, vol. 67, pp. 101–122, Mar. 2019, doi: 10.1016/.j.apm.2018.10.019.

[40] Z. Wu and D. Yu, "Application of improved bat algorithm for solar PV maximum power point tracking under partially shaded condition," *Appl. Soft Comput.*, vol. 62, pp. 101–109, Jan. 2018, doi: 10.1016/.j.asoc.2017.10.039.

[41] W.-C. Hong, M.-W. Li, J. Geng, and Y. Zhang, "Novel chaotic bat algorithm for forecasting complex motion of floating platforms," *Appl. Math. Model.*, vol. 72, pp. 425–443, Aug. 2019, doi: 10.1016/j.apm.2019.03.031.

[42] D. Liu, D. Niu, and H. Wang, "Short-term wind speed forecasting using wavelet transform and support vector machines optimized by genetic algorithm," *Renew. Energy*, vol. 62, pp. 592–597, Feb. 2014, doi: 10.1016/.j.renene.2013.08.011.

[43] H. Liu, C. Chen, H. Tian, "A hybrid model for wind speed prediction using empirical mode decomposition and artificial neural networks," *Renew. Energy*, vol. 48, pp. 545–556, Dec. 201, doi: 10.1016/j.renene.2012.06.012.

[44] C. Ren, N. An, J. Wang, L. Li, B. Hu, and D. Shang, "Optimal parameters selection for BP neural network based on particle swarm optimization: A case study of wind speed forecasting," *Knowl.-Based Syst.*, vol. 56, pp. 226–239, Jan. 2014, doi: 10.1016/j.knosys.2013.11.015.

[45] X. Niu and J. Wang, "A combined model based on data preprocessing strategy and multi-objective optimization algorithm for short-term wind speed forecasting," *Appl. Energy*, vol. 241, pp. 519–539, May 2019, doi: 10.1016/j.apenergy.2019.03.097.

SIZHOU SUN was born in Hexian, China, in 1976. He received the B.Sc. degree in power electronics and power drive from the Anhui University of Technology, China, in 2006. He is currently pursuing the Ph.D. degree with the School of Mechatronic Engineering and Automation, Shanghai University. He is the author of more than ten articles. His research interests include multi-step-ahead time series forecasting, microgrid dispatching, and application of artificial intelligent methods.

JINGQI FU received the B.Sc. degree from the Northeast Heavy Machinery Institute, in 1984, the M.Sc. degree from Yanshan University, in 1989, and the Ph.D. degree from the Nanjing University of Science and Technology, in 1995. He is currently a Professor with Shanghai University. His current research interests include network measurement and control technology.

LISHENG WEI was born in Chaohu, in 1978. He received the Ph.D. degree in control science and engineering from Shanghai University, in 2009. He has been a Professor with the School of Electrical Engineering, Anhui Polytechnic University. He is the author of more than 70 articles. He holds 11 patents. His research interests include image recognition and application, embedded instrumentation and systems, intelligent network control theory, systems and simulation, and data fusion.

ANG LI received the B.Sc. degree from Shanghai University, Shanghai, China, in 2013, where she is currently pursuing the Ph.D. degree in control science and engineering. Her research interests include positioning in wireless networks, algorithm optimization, and neuro-engineering.